Group birefringence cancellation in highly birefringent photonic crystal fibre at telecommunication wavelengths

Philippe Morin, Bertrand Kibler, Julien Fatome, Christophe Finot, Guy Millot

Group modal birefringence inversion in a highly birefringent nonlinear photonic crystal fibre at telecommunication wavelengths

P. Morin, B. Kibler, J. Fatome, C. Finot, G. Millot

Authors' affiliations:

P. Morin, B. Kibler, J. Fatome, C. Finot, G. Millot

Laboratoire Interdisciplinaire Carnot de Bourgogne, UMR 5209 CNRS-Université de Bourgogne, Dijon, FRANCE.

Contact Author: B. Kibler

Contact Address: Laboratoire Interdisciplinaire Carnot de Bourgogne

CNRS UMR 5209

9 Avenue Alain Savary, BP 47 870

21078 Dijon

FRANCE

Fax: +33 (0)3 80 39 59 71

Phone: +33 (0)3 80 39 59 32

Email: Bertrand.Kibler@u-bourgogne.fr

Abstract

We study both numerically and experimentally the spectral dependence of the group modal birefringence in a highly birefringent nonlinear photonic crystal fibre. We demonstrate the possible sign inversion of the group modal birefringence and its cancellation in the telecommunication window corresponding to zero polarization mode dispersion. Two simple experimental techniques are used to evaluate the wavelength of zero group modal birefringence. The experimental results are in excellent agreement with numerical calculations based on vectorial beam propagation method simulations.

Introduction: Since their emergence in the past decade, photonic crystal fibres (PCF) have stimulated major progresses in linear and nonlinear guided optics by offering an outstanding flexibility in the design of the group-velocity dispersion and nonlinear characteristics [1]. Birefringence properties can also be precisely tailored and extremely high built-in birefringence has been reported by breaking the standard perfect sixfold symmetric core and cladding structure [1]. Such polarization-maintaining (PM) PCFs have been decisive for several fibre-based applications such as lasers, interferometers and supercontinuum sources [2-4]. However, several works have stressed that the induced form birefringence characteristics in such PCFs may exhibit a strong wavelength dependence [5], leading to significant variations of the group modal birefringence over a short wavelength range. Recently, Martynkien et al. have also demonstrated that group birefringence can cross zero value near 880 nm in highly birefringent (HB) microstructured fibre with elliptical GeO_2 doped inclusion in the core [6]. In addition, numerical investigations have shown that complex PCFs with composite form and stress birefringence are convenient to manage the wavelength dependence of both phase and group birefringence [7].

In the present work, we describe for the first time the possible inversion of the sign of the group modal birefringence in the telecommunication window by using a commercially available standard HB-PCF. With the help of two simple experimental techniques, we demonstrate a zero value of group modal birefringence (zero polarization mode dispersion) near 1570 nm, i.e. across this wavelength the sign of group birefringence changes. From comparison with numerical simulations, we are able to validate these experimental results, thus having important consequences for the design of PCF-based devices that rely on polarization-dependent nonlinear effects.

The basic parameters required to investigate light propagation in HB PCF, are the phase birefringence $B = (n_{eff,x} – n_{eff,y})$, and the group birefringence $G = (n_{g,x} – n_{g,y}) = B – \lambda\, dB/d\lambda$, where λ is the wavelength, $n_{eff,x}$, $n_{eff,y}$ and $n_{g,x}$, $n_{g,y}$ are the effective refractive indices and the group indices of both orthogonal polarization modes, respectively. In our

experiments, the measurements of group modal birefringence G at telecommunications wavelengths have been achieved using two different methods depicted in Fig. 1. The first setup is based on a frequency domain interferometer using a broadband source. In this case, two polarization modes are first excited at the input and then interfere at the output of the tested fibre due to the polarizer-analyzer device aligned at 45° with respect to the fibre polarization axes. Spectral interferences are recorded using an optical spectrum analyzer (OSA), as shown in Fig. 2(a-b). The second setup relies on the direct analysis of the output state of polarization (SOP) using a commercial polarization analyzer based on the Jones Matrix Eigen-analysis measurement method. In this case, we observe the polarization state evolution on the Poincaré sphere with the scanned input wavelength from a tuneable continuous wave (CW) laser, as shown in Fig. 3(a-c). As a result, the group birefringence was measured by using the so-called wavelength scanning method [8] in both interferometric and polarimetric techniques. The phase difference introduced between two successive maxima spaced by $\Delta\lambda$ on the interference spectrum and by one revolution on the Poincaré sphere is exactly equal to 2π, i.e. the SOP is restored. Consequently, the absolute value of G is directly calculated from the following relation: $|G| = \lambda^2 / (L\,\Delta\lambda)$, where λ is an average wavelength between two successive interference fringes and L is the fibre length. Note that the sign of G can not be determined by means of our setups.

The investigated fibre is a commercially available polarization-maintaining highly nonlinear PCF (Crystal Fibre NL-PM-750) which is generally aimed at near-infrared supercontinuum generation [9]. The fibre length used was 1.42 m. The experimental measurements of the group birefringence are summarized in Fig. 2(c). An remarkable agreement between the two techniques is observed (the comparison was limited to the operating range of the tuneable CW laser). The wavelength dependence of G is significant, as readily assessed by the rapidly varying period of the spectral interferences shown in Fig. 2(a). The most striking feature is however that the absolute value of G cancels at a specific wavelength near 1570 nm. In other words, at 1571.5 nm, the PCF

under investigation exhibits a zero group birefringence. We underline that this zero polarization mode dispersion does not involve a zero phase birefringence. Note also that this zero group birefringence wavelength can be directly retrieved from the symmetry wavelength of the spectral interferences (Fig. 2(a)).

Such a zero value could be linked to a change of sign of the group birefringence. In order to get further insights, we show the wavelength scanning around 1570 nm for the polarimetric method in Fig. 3(b). In this case, the polarization trajectory on the Poincaré sphere does not follow a standard rotation such as the one illustrated in Fig. 3(a); it undergoes an unusual direction inversion during the wavelength scanning. Indeed, we note that the clockwise circular path (Fig 3(a)) becomes anticlockwise (Fig 3(b)) when the wavelength scanning is carried out beyond the zero group birefringence wavelength. This feature definitively confirms our hypothesis: across a particular wavelength the sign of group birefringence changes.

In order to emphasize the remarkable specificity of birefringence characteristics of this HB-PCF, we report in Fig. 2(b,d) the measurements of G for a standard PM fibre based on stress elements (1.12 m long commercial patch cord). As expected, the group birefringence remains constant at all wavelengths (i.e., the period of spectral interferences does not depend on the wavelength) since both phase and group birefringence parameters coincide ($G \approx B$) [5].

In the final section, we present the numerical results of birefringence characteristics obtained by using vectorial beam propagation method simulations [10]. The microstructure parameters used for the numerical simulations were extracted from the data sheet of the PCF [9] and slightly adapted from the SEM image of the fibre cross-section shown in the inset of Fig. 4(a). In particular, this PCF exhibits two large holes on either side of the core. This core asymmetry then involves distinct propagation parameters for the fundamental linearly polarized modes. Our fibre microstructure modelling allows us to calculate the group velocity dispersion (GVD) for both polarization axes of our HB-PCF. These numerical results are in good agreement with that provided by manufacturer, as shown in

Fig. 4(a). The numerical calculations of phase and group birefringence are then reported in Fig. 4(b,c), respectively. Here, the axis along which the mode index is smaller, i.e. the fast axis, corresponds to the x-axis where one finds both large holes. The phase birefringence B increases as the wavelength increases, since the mode field diameter becomes larger resulting in a modal asymmetry growth. Contrary to the phase birefringence, the group birefringence G follows a completely different evolution with wavelength. From our simulations, we can first notice that B and G have opposite signs at low wavelengths, which is simply due to the fact that B/λ is smaller than $dB/d\lambda$. Then, since the phase birefringence increases with wavelength, one can reach a specific wavelength at which the previous terms compensate each other, i.e. G=0. The numerical zero group birefringence is given at 1570 nm. For longer wavelengths, B and G have now the same signs; B/λ became larger than $dB/d\lambda$. We also compare in Fig. 4(b) the numerical values of G with the previous experimental results, and we clearly observe an excellent agreement which confirms the sign inversion of the group modal birefringence and its cancellation in the telecommunication window.

Conclusion: These results therefore demonstrate that high phase birefringence PCF can exhibit both zero polarization mode dispersion and group birefringence inversion at telecommunication wavelengths by using a careful controlled core design. This observation is clearly of interest in the applicability of a novel class of controlled birefringence PCF for nonlinear optics applications. Moreover, it will be also advantageous when the suppression of polarization-dependent nonlinearities is desirable.

Acknowledgements: This work was supported by the Agence Nationale de la Recherche (ANR SOFICARS and PERSYST II projects: ANR-07-RIB-013-03 and ANR-07-TCOM-014).

References

1. P. St. J. Russell, "Photonic-Crystal Fibers," Journal of Lightwave Technology **24**, 4729-4749 (2006).
2. F. C. McNeillie, E. Riis, J. Broeng, J. R. Folkenberg, A. Petersson, H. Simonsen, C. Jacobsen, "Highly polarized photonic crystal fiber laser," Optics Express **12**, 3981-3987 (2004).
3. C. L. Zhao, X. F. Yang, C. Lu, W. Jin, M. S. Demokan, "Temperature-insensitive interferometer using a highly birefringent photonic crystal fiber loop mirror," IEEE Photonics Technology Letters **16**, 2535-2537 (2004).
4. C. Xiong, W. J. Wadsworth, "Polarized supercontinuum in birefringent photonic crystal fibre pumped at 1064 nm and application to tuneable visible/UV generation," Optics Express **16**, 2438-2445 (2008).
5. M. Legre, M. Wegmuller, N. Gisin, "Investigation of the ratio between phase and group birefringence in optical single-mode fibers," Journal of Lightwave Technology **21**, 3374-3378 (2003).
6. T. Martynkien, M. Szpulak, G. Statkiewicz-Barabach, J. Olszewski, A. Anuszkiewicz, W. Urbanczyk, K. Schuster, J. Kobelke, A. Schwuchow, J. Kirchhof, H. Bartelt, "Birefringence in microstructure fiber with elliptical GeO_2 highly doped inclusion in the core," Optics Letters **33**, 2764-2766 (2008).
7. A. Tonello, S. Wabnitz, T. Martynkien, G. Golojuch, W. Urbanczyk, "Control of modulation and soliton polarization instabilities in photonic crystal fibers with birefringence management," Optical Quantum Electronics **39**, 435-453 (2007).
8. S. C. Rashleigh, "Wavelength dependence of birefringence in highly birefringent fibers," Optical Letters **7**, 294-296 (1982).
9. NKT Photonics, "Nonlinear Photonic Crystal Fiber - NL·PM·750 - Data sheet,"

http://www.nktphotonics.com/files/files/datasheet_nl-pm-750.pdf.

10. BeamPROP 8.1 (RSoft Design Group, New York, 2008).

Figure Captions:

Fig. 1 Experimental setups based on (a) the interferometric method and (b) the polarimetric method used for group modal birefringence measurements. All the symbols have their usual meaning. (P: polarizer, A: analyzer, SMF: single mode fiber, FUT: fibre under test).

Fig. 2 (a,b) Experimental spectral interferences obtained with the first setup for our HB-PCF and the standard PM fibre, respectively. (c,d) Comparison of experimental results of group birefringence measurement obtained with both methods for our HB-PCF and the standard PM fibre, respectively.

Fig. 3 Evolution of Stokes vector on the Poincaré sphere of the SOP obtained at the HB-PCF output with the second experimental setup and by scanning in the following wavelength ranges: (a) 1540 - 1546.6 nm, (b) 1560 - 1581.8 nm, and (c) 1590 - 1597.4 nm. The initial and final wavelengths of each scanning are indicated by a cross and a circle, respectively. The trajectory direction is also indicated by an arrow.

Fig. 4 (a) Numerical dispersion calculations of both fundamental orthogonal polarized modes of our HB-PCF performed from the SEM image of the fibre cross section (inset) compared to manufacturer data. (b) Numerical calculation of the phase modal birefringence B. (c) Numerical calculation of the group modal birefringence G compared to our experimental results obtained in the telecommunication window.

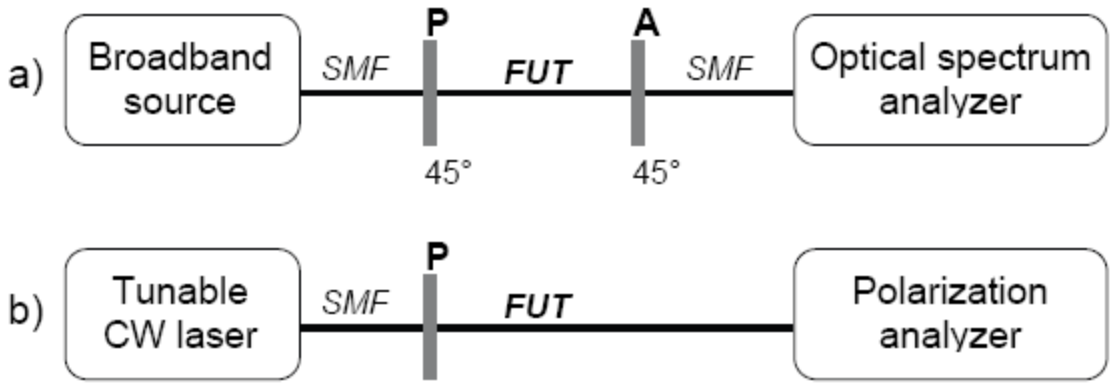
a)
Broadband source
SMF
P
FUT
A
SMF
Optical spectrum analyzer
45°
45°
b)
Tunable CW laser
SMF
P
FUT
Polarization analyzer

FIGURE 1

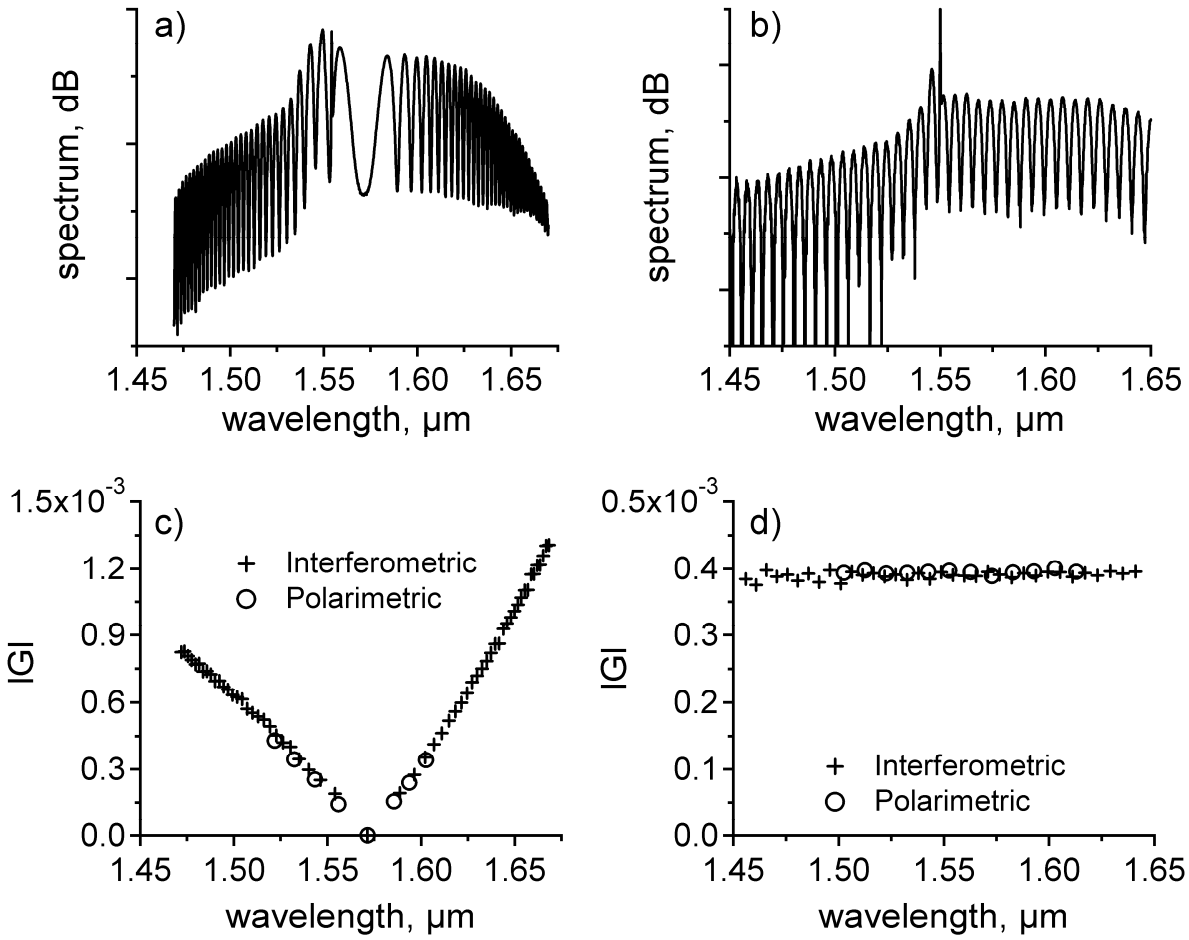
a)
spectrum, dB
1.45 1.50 1.55 1.60 1.65
wavelength, μm
b)
spectrum, dB
1.45 1.50 1.55 1.60 1.65
wavelength, μm
1.5x10-3
c)
Interferometric
Polarimetric
IGI
1.2
0.9
0.6
0.3
0.0
1.45 1.50 1.55 1.60 1.65
wavelength, μm
0.5x10-3
d)
IGI
0.4
0.3
0.2
0.1
0.0
Interferometric
Polarimetric
1.45 1.50 1.55 1.60 1.65
wavelength, μm

FIGURE 2

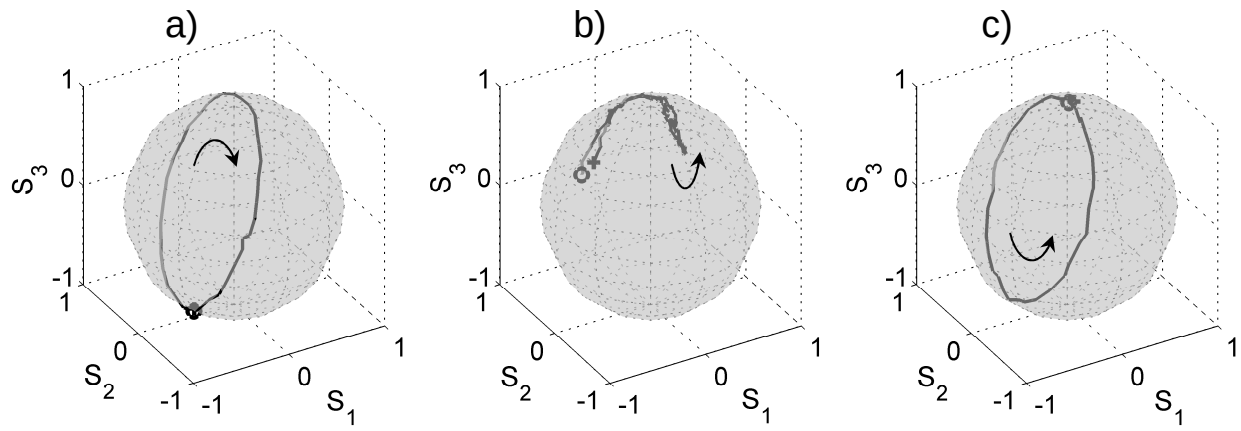

FIGURE 3

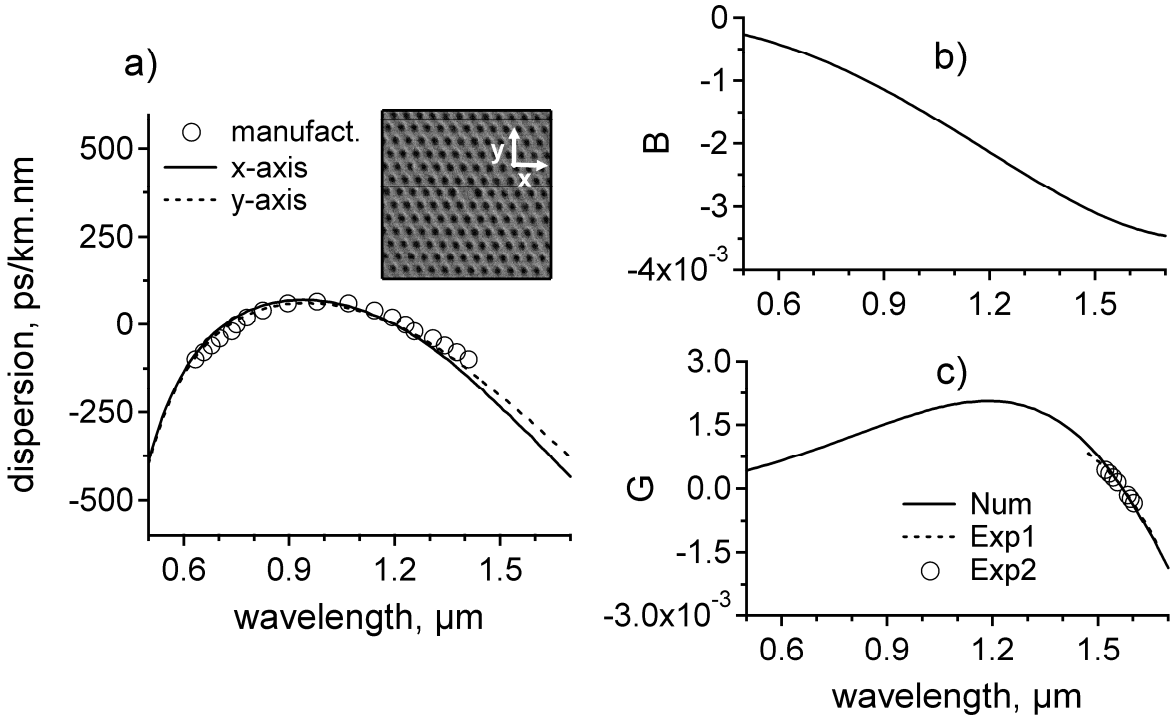
a)
manufact.
x-axis
y-axis
y
x
dispersion, ps/km.nm
500
250
0
-250
-500
0.6
0.9
1.2
1.5
wavelength, μm
b)
B
0
-1
-2
-3
-4x10-3
0.6
0.9
1.2
1.5
c)
G
3.0
1.5
0.0
-1.5
-3.0x10-3
Num
Exp1
Exp2
0.6
0.9
1.2
1.5
wavelength, μm

FIGURE 4